RSC Advances

PAPER

View Article Online
View Journal | View Issue

Open Access Article. Published on 19 May 2022. Downloaded on 10/22/2025 12:56:45 AM.
This article is licensed under a Creative Commons Attribution-NonCommercial 3.0 Unported Licence.

Check for updates

Cite this: *RSC Adv.*, 2022, **12**, 15354

Vanadium nitride nanoparticle decorated N-doped carbon nanotube/N-doped carbon nanosheet hybrids *via* a C_3N_4 self-sacrificing method for electrochemical capacitors†

Jinghua Liu,[a] Xiong He,*[a] Fei Guo,[a] Baosheng Liu,[a] Zijun Sun,[a] Li Zhang[a] and Haixin Chang *[b]

Received 3rd May 2022
Accepted 5th May 2022

DOI: 10.1039/d2ra02789e

rsc.li/rsc-advances

Owing to the wide negative potential window (~1.2 V) along with high specific capacitance (1340 F g^{-1}) in alkaline electrolyte, vanadium nitride (VN) has been served as promising negative supercapacitor electrode material. However, VN is easy to dissolve during cycling process and shows low capacitance retainability. Herein, a hybrid electrode (marked as VN/NCNT/NCN), featuring VN nanoparticles and N-doped carbon nanotube inserted in N-doped carbon nanosheets, has been fabricated with a facile C_3N_4 self-sacrificing method. The porous structure and high conductive carbon skeleton, as well as the uniform distribution of VN nanoparticles give VN/NCNT/NCN a great amount of active site and fulfill excellent electrochemical performance for VN/NCNT/NCN-based electrode. The as-fabricated hybrid electrode exhibits a maximum specific capacitance of 232.9 F g^{-1} at 1 A g^{-1}. Moreover, the cycling performance has been greatly improved and the specific capacitance remains 91% after 5000 cycles.

Introduction

The growing consumption of natural energy and the consequent environmental problems have triggered efforts to explore clean and sustainable resources.[1–3] Supercapacitors (SCs), as a promising candidate for energy storage, have been intensively studied because of the high power density and long life span.[4–6] The electrochemical performance of SCs is greatly influenced by the capacitive performance of electrode material, which is generated by the electric double layer capacitance (EDLC) and/or pseudocapacitance.[7,8] In EDLCs, energy storage involves a non-faradaic process along with ion adsorption on the electrode/electrolyte. Nevertheless, the unsatisfied specific capacitance of EDLCs electrode material restricts the development of SCs. Pseudocapacitive electrode materials accumulate electron through fast reversible surface redox reactions and obtain high specific capacitance.

Vanadium nitride (VN)-based supercapacitor electrode demonstrates a highest mass specific capacitance of 1340 F g^{-1}.[9] Moreover, VN fulfills appropriate negative potential working window and good electron conductivity, which makes it charming negative electrode materials.[10,11] But the SCs constructed with VN electrode suffer from poor stability in aqueous electrolytes, because VN is easy to be oxidized.[9] In order to improve their stability, great efforts have been devoted to protect VN from oxidizing, involving heteroatoms doping to stabilize VN intrinsic structure and coating protective shells on VN. Various protective shells have been coated on the VN surface, such as metal oxides, conductive polymers, and carbon materials.[12–14] Among them, carbon shells are highly conductive and capable of fast ion transport. For instance, Bhat *et al.* fabricated porous graphene using an eco-friendly procedure, which can be used as promising supercapacitor electrode material.[15] Moreover, carbon-based materials, combined the advantages of carbon materials and pseudocapacitive materials, have been intensively synthesized. Bhat *et al.* synthesized porous graphene–NiO nanocomposites again *via* a simple solvothermal approach and applied to supercapacitor, which presented good capacitance performance and high cyclic stability.[16] Except for metal-oxides, lots of VN/carbon nanocomposites have been fabricated and achieved enhanced electrochemical performance.[17–19]

Recently, C_3N_4 was chosen as N-doped source for preparation of N-doped carbon materials.[20,21] In addition, C_3N_4 can also be used for the synthesis of nitrides, such as VN, TiN, MoN *et al.*[22–25] During these processes, C_3N_4 decomposes under high temperature and is easy to eliminate. Based on this, C_3N_4 can behave as a self-sacrificing template for preparing the hybrids of nitrides and N-doped carbon materials. For example, Xing *et al.*

[a]*School of Microelectronics and Materials Engineering, Guangxi University of Science and Technology, Liuzhou 545000, China*

[b]*Quantum-Nano Matter and Device Lab, State Key Laboratory of Material Processing and Die & Mould Technology, School of Materials Science and Engineering, Huazhong University of Science and Technology, Wuhan 430074, China*

† Electronic supplementary information (ESI) available. See https://doi.org/10.1039/d2ra02789e

© 2022 The Author(s). Published by the Royal Society of Chemistry

Open Access Article. Published on 19 May 2022. Downloaded on 10/22/2025 12:56:45 AM.
This article is licensed under a Creative Commons Attribution-NonCommercial 3.0 Unported Licence.

fabricated vanadium nitride/nitrogen-doped carbon composite materials by utilizing C_3N_4 as eco-friendly nitrogen source and applied the materials for supercapacitors, which exhibited favorable specific capacitance and cycling stability.[26] According to the previous reports, carbon nanotubes (CNTs) can insert into the carbon nanosheets to fabricate a 3D porous structure. The inserted CNT could effectively inhibit the aggregation of carbon nanosheets and further enhance conductivity.[27,28]

Inspired by this structure, a facile and efficient C_3N_4 template method is used to fabricate N-doped carbon nanosheets (NCNs) inserted with N-doped CNT (NCNT) and VN nanoparticles (VN/NCNT/NCN). As a sacrificial template, C_3N_4 not only functions as C and N sources for the preparation of VN/NCNT/NCNs, but also creates plenty of pores among the carbon skeleton. The porous structure of VN/NCNT/NCN and the decoration of VN, as well as the doping N elements give VN/NCNT/NCN a great amount of active site. Moreover, NCNTs linked with carbon nanosheets fulfill electrode materials fast electron transport and ion transfer. When used for supercapacitor electrode material in 6 M KOH aqueous electrolyte, the specific capacitance of 232.9 F g^{-1} can be obtained for VN/NCNT/NCN electrode at 1 A g^{-1}. Furthermore, the unique structure greatly improves its cycling stability. After 5000 cycles at 10 A g^{-1}, VN/NCNT/NCN electrode maintains 91% of the initial capacitance. Moreover, the possible formation mechanism of the hybrids was discussed.

Experimental

Materials

Dicyandiamide (DCDA, 99%), potassium hydroxide (KOH, 95%), and ethyl alcohol (95%) were purchased from Aladdin Chemical (China). Vanadium(IV) sulfate oxide hydrate ($VOSO_4$, 99.9%) was purchased from Alfa Aesar. Polytetrafluoroethylene (PTFE, 60%) was purchased from Daikin corporation. Carbon black (98%) was purchased from Lion corporation. Carbon nanotube (CNT, 95%) was purchased from Xfnano corporation. Ni foam (99.9%) was purchased from Lizhiyuan corporation. All chemical reagents were used directly without further purification.

Synthesis of VN/NCNT/NCN hybrids

The synthesis of VN/NCNT/NCN hybrids were fabricated as follows. Briefly, 1 g of DCDA, 0.01 g of CNT, and a certain amount of $VOSO_4$ were mixed together and grinded into uniform powder. With heating step of 5 °C min^{-1}, straight calcination of the mixture was applied at 550 °C for 4 h under N_2 flow. Then, with increasing the temperature to 800 °C and keeping for another 2 h, the final products were obtained. The amount of $VOSO_4$ was 0.02 g, 0.05 g and 0.08 g. The corresponding samples were marked as VN/NCNT/NCN-1, VN/NCNT/NCN-2, and VN/NCNT/NCN-3, respectively. In addition, a mixture without $VOSO_4$ was adopted *via* a similar synthesis method to prepare NCNT/NCN nanocomposite for comparison. Pure VN nanoparticles were fabricated under NH3 atmosphere at same heating step.

Material characterization

The phases of different nanocomposites were investigated by X-ray diffractometer (XRD, Ultima IV, RIGAKU) with Cu-Kα radiation ($\lambda = 0.1504$ nm). The morphologies of the samples were captured by scanning electron microscope (SEM, Gemini 300, Zeiss) and transmission electron microscope (TEM, Tecnai TF20, FEI). Thermogravimetric analysis was conducted on an analysis instrument (Discovery TGA5500, USA) under N_2 atmosphere with heating step of 5 °C min^{-1}. Nitrogen adsorption/desorption isotherms were obtained on (AUTOSORB-IQ-MP, Quantachrome) to analysis the pore size distribution with Barret–Joyner–Halenda (BJH) model and specific surface area with Brunauer–Emmett–Teller (BET) equation. The element content and composition on the surface of samples were carried out on X-ray photoelectron spectroscope (XPS, Scientific K-Alpha+, Thermo fisher). Fourier transform infrared (FT-IR) spectrum was performed with a Nicolet 50 spectrometer.

Electrochemical measurements

To prepare the working electrodes, a slurry made of active materials, carbon black, and polytetrafluoroethylene with a mass ration of 8 : 1 : 1 was spreaded on nickel foam (1 cm × 1 cm). After drying at 100 °C, the working electrode was pressed into pieces. All the electrochemical performance, including cyclic voltammetry (CV), galvanostatic charge/discharge (GCD), and electrochemical impedance spectroscopy (EIS) were carried out with a three-electrode system in 6 M KOH aqueous solution. A Pt foil electrode and a Hg/HgO electrode were used as the counter electrode and reference electrode, respectively. The specific capacitance (C_s, F g^{-1}) of the as-prepared electrode materials was calculated from the discharge curve of GCD according to the following equation.

$$C_S = \frac{I \times \Delta t}{m \times \Delta V}$$

where, I (A) is the discharge current, Δt (s) represents the discharge time, m (g) is the mass of the active material, and ΔV (V) is the voltage change during the discharge process.

Results and discussion

Synthesis mechanism of VN/NCNT/NCN hybrids

The synthesis of VN/NCNT/NCN nanocomposites was adopted a two-step pyrolysis process, as shown in Scheme 1. At first, DCDA was condensed into C_3N_4 at 550 °C and $VOSO_4$ was decomposed into vanadium oxide (VO_x) at the same time. When the temperature increased up to 700 °C, C_3N_4 decomposed

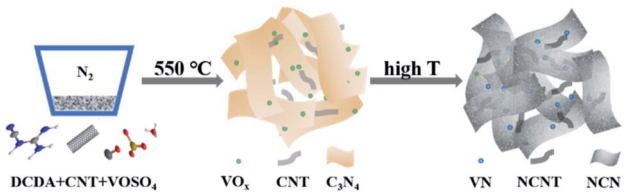

Scheme 1 Scheme for the synthesis of VN/NCNT/NCN hybrids.

Open Access Article. Published on 19 May 2022. Downloaded on 10/22/2025 12:56:45 AM.
This article is licensed under a Creative Commons Attribution-NonCommercial 3.0 Unported Licence.

thoroughly, which produced lots of small molecules with N atom and C atom.[29] After rearrangement of N, C atoms, N-doped carbon nanosheets were left, along with the introduction of N atom into CNT and formation of N-doped CNT. Besides, the transformation of VO_x to VN was occurred in this stage.[30] Finally, the hybrid consisted with NCN, NCNT, and VN was fabricated. This phenomenon was evidenced through the TGA curves in Fig. 1a. After calcination, CNT shows no mass loss but DCDA totally decomposes. $VOSO_4$ decomposed before 600 °C and simultaneously reacted with the small N-rich molecules. At last, VN nanoparticles, NCNT along with NCN were left and their hybrid product was formed.

The intermediate synthesized at 550 °C was investigated by XRD, FTIR, and SEM in Fig. 1b–d. As presented in Fig. 1b, the Bragg diffraction peak located at 27.3° corresponds to the (002) plane of C_3N_4.[31,32] In addition, the FT-IR spectrum further shows the evidence of C_3N_4. The characteristic peak at 807.5 cm^{-1} is corresponding to the triazine breathing vibration. Several peaks located at the range of 1200–1600 cm^{-1} come from the typical C=N, C–N bond in the triazine (C_6N_7) ring.[33] The peak noticed around 3400 cm^{-1} is related to vibrational mode of N–H/O–H surface-active species. These results indicate the presence of C_3N_4 at 550 °C. The SEM image of the intermediate showed obvious bulk morphology of C_3N_4, with randomly dispersed particles on the surface. All these results demonstrate the formation of C_3N_4 intermediate, which was further used to regulate the fabrication of VN/NCNT/NCN hybrids.

Morphologies and structures of VN/NCNT/NCN hybrids

The XRD patterns were performed to verify the successful preparation of VN/NCNT/NCN hybrids. As shown in Fig. 2a, pure VN exhibits typical diffraction peaks at 37.9°, 44.1°, 64.0°, and 76.8°, corresponding to (111), (200), (220), and (311) plane of VN (PDF#35-0768).[13,34] The VN/NCNT/NCN hybrids also show these characteristic peaks. At the same time, a distinct peak at 26.4° from (002) plane of carbon skeleton can be seen,

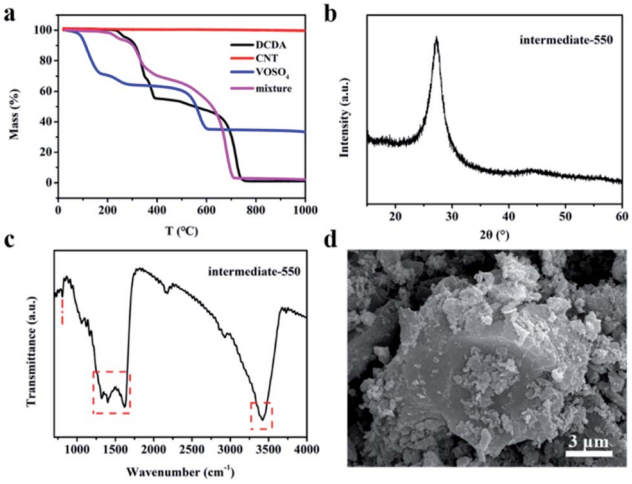

Fig. 1 (a) TGA curves of DCDA, CNT, $VOSO_4$, and the mixture. (b) XRD pattern. (c) FT-IR spectrum. (d) SEM image of the intermediate calcinated at 550 °C.

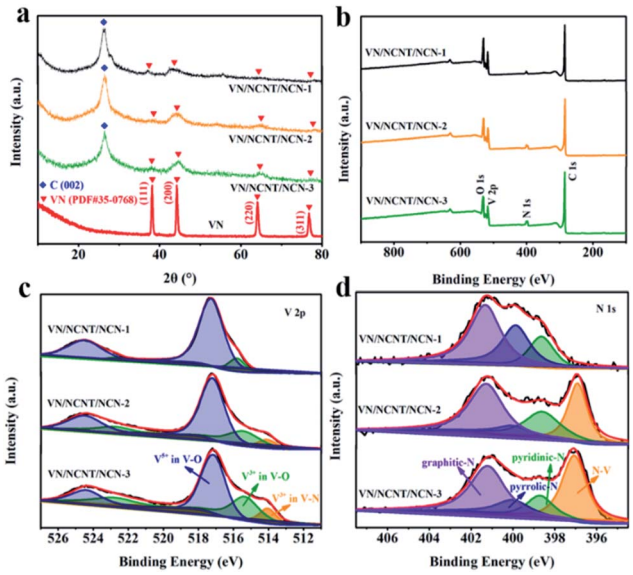

Fig. 2 (a) XRD patterns of VN and VN/NCNT/NCN hybrids. (b) XPS spectra of VN/NCNT/NCN hybrids. (c) V 2p XPS spectra. (d) N 1s XPS spectra.

suggesting the hybrid structure of carbon material with VN. Moreover, the temperature greatly influences the structure of VN/NCNT/NCN. With the increasing temperature, the peak intensity of VN gradually increases, but the (002) peak of carbon slightly decreases, indicating the increased crystallinity of VN.

The XPS survey spectra of VN/NCNT/NCN indicate the presence of C, O, N, and V elements (Fig. 2b). As presented in Table 1, the C and V element in the hybrids calcinated at 800 °C shows similar atomic ratio. But the N element content gradually increased with the increasing content of $VOSO_4$, indicating that V atom captures more N atom. Fig. 2c and d show the high-resolution peak of V 2p and N1s. For V 2p spectra, the peaks centered at 517.2 eV and 524.4 eV can be assigned to V^{5+} in V–O bond, while the peaks at 515.3 eV and 522.5 eV belong to V^{3+} in V–O bond. The peak at 514.0 eV and 520.1 eV can be attributed to VN.[25] The N 1s spectra show four separated peaks related with graphitic-N (401.2 eV), pyrrolic-N (399.9 eV), pyridinic-N (398.7 eV), and V–N bonds (397.1 eV).[35,36] The V–N bond in V 2p and N 1s spectra further demonstrates the successful formation of VN by the template sacrificing method. With the increasing amount of $VOSO_4$, the content of V–N bond in V 2p and N 1s spectra obviously increases, which is in agreement with the XRD results.

N_2 adsorption and desorption isotherms of VN/NCNT/NCN were displayed in Fig. 3a. Typical type-IV isotherm with the

Table 1 XPS results and SSA of VN/NCNT/NCN hybrids

Sample	C (at%)	N (at%)	O (at%)	V (at%)	S_{BET} (m^2 g^{-1})
VN/NCNT/NCN-1	66.39	3.04	18.63	11.94	226.8
VN/NCNT/NCN-2	67.77	5.79	15.49	10.95	183.2
VN/NCNT/NCN-3	67.87	6.52	15.19	10.43	143.3

 © 2022 The Author(s). Published by the Royal Society of Chemistry

Open Access Article. Published on 19 May 2022. Downloaded on 10/22/2025 12:56:45 AM.
This article is licensed under a Creative Commons Attribution-NonCommercial 3.0 Unported Licence.

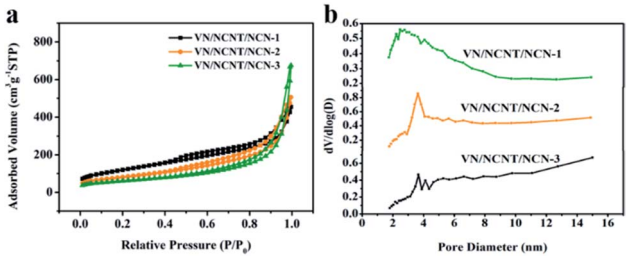

Fig. 3 (a) Nitrogen adsorption/desorption isotherms. (b) Pore size distribution of VN/NCNT/NCN hybrids.

hysteresis loop represents the mesoporous structure of VN/NCNT/NCN hybrids. The corresponding specific surface areas of VN/NCNT/NCN-1, VN/NCNT/NCN-2, and VN/NCNT/NCN-3 (in Table 1) are 226.8 $m^2\ g^{-1}$, 183.2 $m^2\ g^{-1}$, and 143.3 $m^2\ g^{-1}$. The increasing amount of $VOSO_4$ results in the accumulation of VN nanoparticles, further decreasing the specific surface area of VN/NCNT/NCN hybrids. Simultaneously, pore size distribution curves are demonstrated in Fig. 3b and further verify the porous structure.

The morphology of VN/NCNT/NCN-2 was observed with SEM and TEM images. As exhibited in Fig. 4a–c, VN/NCNT/NCN-2 exhibits layered structure with plenty of nanoparticles dispersed on its surface. The corresponding element mapping represents uniform distribution of C, N, O, and V elements. TEM and HRTEM images reveal more details about VN/NCNT/NCN hybrids in Fig. 4d–f. It can be seen that tubular structure inserts into the layered carbon sheet and nanoparticles around 5 nm are embedded into the carbon skeleton, forming an interconnected structure. CNT structure combined with layered carbon sheets can be observed more clearly in the TEM images from Fig. S1.† A lattice spacing of 0.206 nm is indexed to the (200) facet of VN, corresponding with XRD and XPS results.[37] This unique structure protects VN nanoparticles from dissolution in aqueous electrolyte, which could improve the cycling stability.

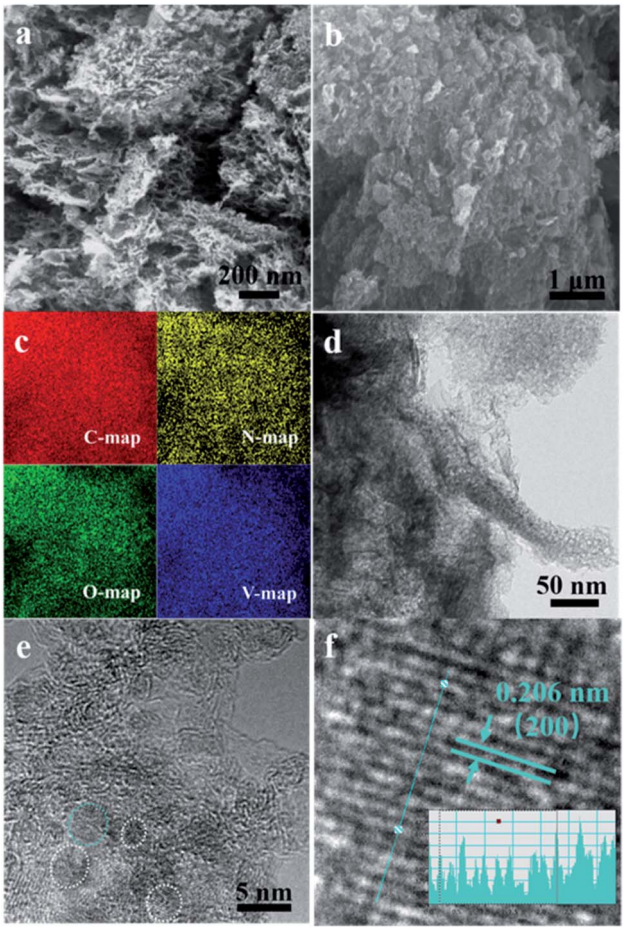

Fig. 4 SEM images (a–c) and TEM images (d–f) of VN/NCNT/NCN-2.

Electrochemical performance

The electrochemical behavior of the as-prepared VN, NCNT/NCN, and VN/NCNT/NCN hybrids was characterized with a three-electrode configuration in 6 M KOH aqueous electrolyte. Fig. 5a depicts the CV curves of VN, NCNT/NCN, and VN/NCNT/NCN hybrids at 10 mV s^{-1}. The different shapes of the CV curves demonstrate their different capacitance characteristics. The CV curve of pure VN exhibits distinct redox peaks at about −0.6/−0.9 V derived from redox processes between V element with different valence. This intensity of redox peaks in VN/NCNT/NCN hybrids decreases significantly and the hybrids exhibit distorted rectangular shapes, due to the capacitance contribution of EDLC from carbon materials. Besides, the NCNT/NCN curve displays a pair of small peaks, which may be ascribed to the impurity in CNT. Moreover, the enlarged CV integral area of the VN/NCNT/NCN-2 than that of VN, NCNT/NCN, VN/NCNT/NCN-1, and VN/NCNT/NCN-3 suggests higher capacitance of VN/NCNT/NCN-2 electrode. The GCD curves of VN, NCNT/NCN, and VN/NCNT/NCN hybrids at 1 A g^{-1} are presented in Fig. 5b. All the curves display triangular shape with slight distortion. From the discharge time curve, it can be seen that the longest discharge time of VN/NCNT/NCN-2 indicates largest capacitance capacity, which agrees well with the CV curves. The specific capacitance of the five samples is 226.8 F g^{-1} (VN/NCNT/NCN-1), 232.9 F g^{-1} (VN/NCNT/NCN-2), 198.0 F g^{-1} (VN/NCNT/NCN-3), 89.0 F g^{-1} (NCNT/NCN), and 135.8 F g^{-1} (VN), respectively.

Fig. 6a presents the CV curves of VN/NCNT/NCN-2 at various scan rate from 5 to 100 mV s^{-1}. The distorted rectangular

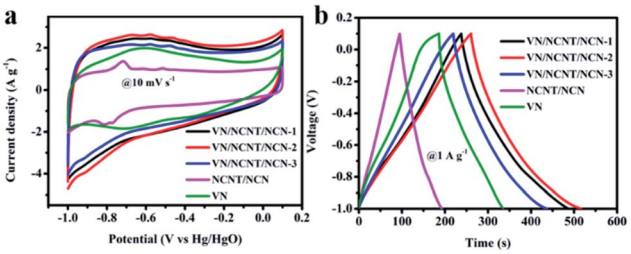

Fig. 5 (a) CV curves at 10 mV s^{-1}. (b) GCD curves at 1 A g^{-1} for VN, NCNT/NCN, and VN/NCNT/NCN hybrids.

Open Access Article. Published on 19 May 2022. Downloaded on 10/22/2025 12:56:45 AM.
This article is licensed under a Creative Commons Attribution-NonCommercial 3.0 Unported Licence.

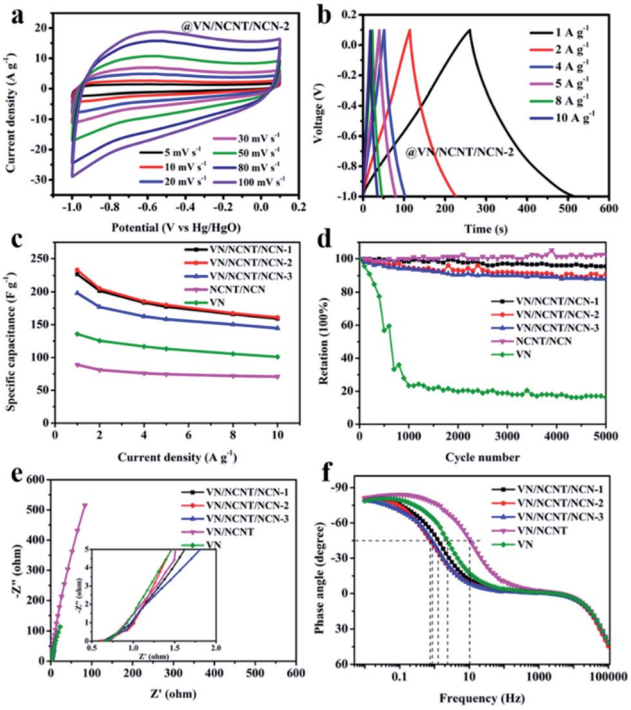

Fig. 6 (a and b) CV curves at different scan rates and GCD curves at different current density of VN/NCNT/NCN-2, (c and d) Specific capacity and cycling performance, (e and f) Nyquist plots and Bode plots of VN, NCNT/NCN, and VN/NCNT/NCN hybrids.

shapes demonstrate EDLC and pseudocapacitance are co-existed in VN/NCNT/NCN-2 electrode. Fig. 6b depicts the GCD curves of VN/NCNT/NCN-2 electrode at various current density. On the basis of discharge time, the specific capacitances of VN/NCNT/NCN-2 electrode are 232.9 F g^{-1} (1 A g^{-1}), 204.9 F g^{-1} (2 A g^{-1}), 185.5 F g^{-1} (4 A g^{-1}), 180.0 F g^{-1} (5 A g^{-1}), 167.3 F g^{-1} (8 A g^{-1}), and 160.9 F g^{-1} (10 A g^{-1}), respectively. Moreover, the specific capacitances of VN, NCNT/NCN, and other VN/NCNT/NCN hybrids are recorded in Fig. 6c. Fig. 6d shows the cycle stability of the five electrodes after 5000 cycles at 10 A g^{-1}. It can be observed that the electrochemical stability of VN/NCNT/NCN hybrids greatly improves compared with the stability of pure VN. After 5000 cycles, the specific capacitance of VN/NCNT/NCN hybrids remains about 95% (VN/NCNT/NCN-1), 91% (VN/NCNT/NCN-2), and 88% (VN/NCNT/NCN-3), respectively. The XRD pattern of VN/NCNT/NCN-2 electrode film (Fig. S2†) has been performed to investigate the phase change after 5000 cycle charge–discharge tests. Typical VN characteristic peaks and many new peaks can be found. And these new peaks are assigned to vanadium oxide or hydroxide, which may still exhibit a part of capacity and lead to the stable electrochemical performance. The good stability may be ascribed to the following reasons. (1) During the cycling process, VN partially converted into vanadium oxide or hydroxide, these materials may still show a part of the capacity and exhibit a satisfying performance.[38] (2) The highly conductive carbon materials could protect VN from dissolution and provide fast ion transfer.[39,40] The cyclic stability of recently reported VN, vanadium-based/carbon hybrids, other supercapacitor electrode materials tested in three-electrode configurations were summarized in Table S1.† It is clear that our sample exhibits relatively good electrochemical stability among these electrode materials, which is close to the stability of metal-oxide/graphene nanocomposites.[41,42]

The EIS plots and Bode plots given in Fig. 6e and f were further performed to reveal the ion/electron transport properties within VN, NCNT/NCN, and VN/NCNT/NCN electrodes. The EIS plots feature a depressed semicircle and a nearly vertical curve. The equivalent series resistance (R_s) of VN/NCNT/NCN electrodes, from the x axis intercept, was calculated to be 0.59 Ω (VN/NCNT/NCN-1), 0.60 Ω (VN/NCNT/NCN-2), 0.63 Ω (VN/NCNT/NCN-3), which is slightly lower than that of VN (0.61 Ω) and NCNT/NCN (0.62 Ω). Besides, at the phase angle of −45°, the characteristic frequency f_0 is 1.28, 0.76, 0.84, 10.58 and 2.34 Hz for VN/NCNT/NCN-1, VN/NCNT/NCN-2, VN/NCNT/NCN-3, NCNT/NCN, and VN. And the relevant time constant τ_0 is 0.12, 0.21, 0.19, 0.02, and 0.07 s, respectively (Fig. 4e). The larger τ_0 values of VN/NCNT/NCN electrodes suggest favorable rate capability of the VN/NCNT/NCN based SCs.

In order to explore the practical application of VN/NCNT/NCN electrode, a symmetrical supercapacitor with sandwich structure was fabricated using VN/NCNT/NCN-2 electrode. Fig. 7a and b show the CV curves and GCD curves of VN/NCNT/NCN-2 based supercapacitor (VN/NCNT/NCN-2-SC) at different scan rates and current densities. The quasi-rectangular shape from CV curves and the nearly triangular shape from GCD curves exhibit excellent capacitive behavior and electrochemical reversibility of VN/NCNT/NCN-2-SC. As calculated in Fig. 7c, the total specific capacitance of VN/NCNT/NCN-2 can reach 43.6 F g^{-1} at 1 Ag^{-1}, which remains 25.5 F g^{-1} at 10 A g^{-1}. Fig. 7d shows the Ragone plot of VN/NCNT/NCN-2-SC. The VN/NCNT/NCN-2-SC delivers an energy density of 7.3 W h kg^{-1} at a power density of 549.8 W kg^{-1} and remains 4.29 W h kg^{-1} at 5515.7 W kg^{-1}.

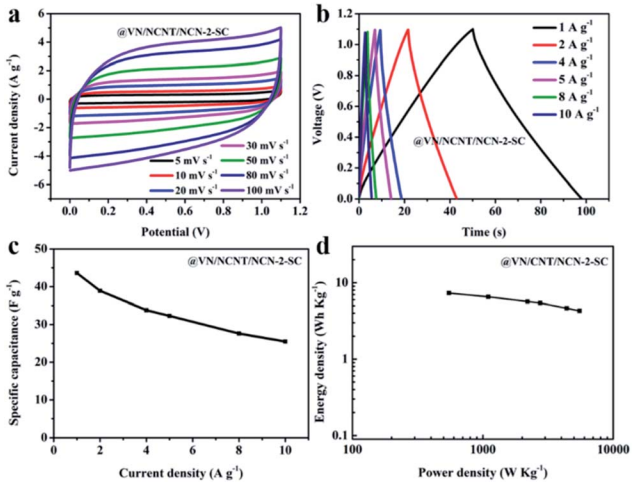

Fig. 7 (a) CV curves of VN/NCNT/NCN-2-SC at different scan rates. (b) GCD curves of VN/NCNT/NCN-2-SC at different current densities. (c) Specific capacitance of VN/NCNT/NCN-2-SC. (d) Ragone plots of VN/NCNT/NCN-2-SC.

 © 2022 The Author(s). Published by the Royal Society of Chemistry

Open Access Article. Published on 19 May 2022. Downloaded on 10/22/2025 12:56:45 AM. This article is licensed under a Creative Commons Attribution-NonCommercial 3.0 Unported Licence.

Conclusion

To sum up, using a facile C_3N_4 self-sacrificing method, the inter-connected VN/NCNT/NCN hybrids were fabricated. The well-designed material features uniform distribution of VN nanoparticles and NCNT, which inserted in the porous carbon sheets. As a promising supercapacitor electrode, the VN/NCNT/NCNT-2 electrode exhibits a maximum specific capacitance of 232.9 F g^{-1} at 1 A g^{-1}. Moreover, after 5000 cycles, the specific capacitance retains 91%, which is superior than that of pure VN electrode. The symmetrical supercapacitor based on VN/NCNT/NCN-2 delivers an energy density of 7.3 W h kg^{-1} at a power density of 549.8 W kg^{-1}, demonstrating promising application in energy storage field.

Conflicts of interest

There are no conflicts to declare.

Acknowledgements

We are grateful for the financial support of this research from the Science and Technology Project of Guangxi (AD19245154 and AD19245104), Natural Science Foundation of Guangxi Province (2021GXNSFBA075025), and Doctoral Fund Project, Guangxi University of Science and Technology (19Z24, 19Z23).

Notes and references

1 N. Kittner, F. Lill and D. M. Kammen, Energy storage deployment and innovation for the clean energy transition, *Nat. Energy*, 2017, **2**, 1–6.
2 H. Li, X. Zhou, W. Zhai, S. Lu, J. Liang, Z. He, H. Long, T. Xiong, H. Sun and Q. He, Phase engineering of nanomaterials for clean energy and catalytic applications, *Adv. Energy Mater.*, 2020, **10**, 2002019.
3 E. Pomerantseva, F. Bonaccorso, X. Feng, Y. Cui and Y. Gogotsi, Energy storage: The future enabled by nanomaterials, *Science*, 2019, 366.
4 Q. L. Wei, F. Y. Xiong, S. S. Tan, L. Huang, E. H. Lan, B. Dunn and L. Q. Mai, Porous One-Dimensional Nanomaterials: Design, Fabrication and Applications in Electrochemical Energy Storage, *Adv. Mater.*, 2017, **29**, 39.
5 T. M. Gur, Review of electrical energy storage technologies, materials and systems: challenges and prospects for large-scale grid storage, *Energy Environ. Sci.*, 2018, **11**, 2696–2767.
6 G. P. Wang, L. Zhang and J. J. Zhang, A review of electrode materials for electrochemical supercapacitors, *Chem. Soc. Rev.*, 2012, **41**, 797–828.
7 C. Choi, D. S. Ashby, D. M. Butts, R. H. DeBlock, Q. L. Wei, J. Lau and B. Dunn, Achieving high energy density and high power density with pseudocapacitive materials, *Nat. Rev. Mater.*, 2020, **5**, 5–19.
8 J. S. M. Lee, M. E. Briggs, C. C. Hu and A. I. Cooper, Controlling electric double-layer capacitance and pseudocapacitance in heteroatom-doped carbons derived from hypercrosslinked microporous polymers, *Nano Energy*, 2018, **46**, 277–289.
9 D. Choi, G. E. Blomgren and P. N. Kumta, Fast and reversible surface redox reaction in nanocrystalline vanadium nitride supercapacitors, *Adv. Mater.*, 2006, **18**, 1178–1182.
10 Z. H. Gao, H. Zhang, G. P. Cao, M. F. Han and Y. S. Yang, Spherical porous VN and NiO_x as electrode materials for asymmetric supercapacitor, *Electrochim. Acta*, 2013, **87**, 375–380.
11 B. Asbani, K. Robert, P. Roussel, T. Brousse and C. Lethien, Asymmetric micro-supercapacitors based on electrodeposited RuO_2 and sputtered VN films, *Energy Storage Materials*, 2021, **37**, 207–214.
12 Q. W. Li, Y. Chen, J. B. Zhang, W. F. Tian, L. Wang, Z. G. Ren, X. C. Ren, X. X. Li, B. Gao, X. Peng, P. K. Chu and K. F. Huo, Spatially confined synthesis of vanadium nitride nanodots intercalated carbon nanosheets with ultrahigh volumetric capacitance and long life for flexible supercapacitors, *Nano Energy*, 2018, **51**, 128–136.
13 M. H. Chen, H. Fan, Y. Zhang, X. Q. Liang, Q. G. Chen and X. H. Xia, Coupling PEDOT on Mesoporous Vanadium Nitride Arrays for Advanced Flexible All-Solid-State Supercapacitors, *Small*, 2020, 16.
14 Y. L. Yang, L. Zhao, K. W. Shen, Y. Liu, X. N. Zhao, Y. G. Wu, Y. Q. Wang and F. Ran, Ultra-small vanadium nitride quantum dots embedded in porous carbon as high performance electrode materials for capacitive energy storage, *J. Power Sources*, 2016, **333**, 61–71.
15 M. Sethi, H. Bantawal, U. S. Shenoy and D. K. Bhat, Eco-friendly synthesis of porous graphene and its utilization as high performance supercapacitor electrode material, *J. Alloys Compd.*, 2019, **799**, 256–266.
16 M. Sethi, U. S. Shenoy and D. K. Bhat, Simple solvothermal synthesis of porous graphene-NiO nanocomposites with high cyclic stability for supercapacitor application, *J. Alloys Compd.*, 2021, **854**, 157190.
17 H. N. Jia, Y. F. Cai, S. Li, X. H. Zheng, L. F. Miao, Z. Y. Wang, J. L. Qi, J. Cao, J. C. Feng and W. D. Fei, In situ synthesis of core-shell vanadium nitride@N-doped carbon microsheet sponges as high-performance anode materials for solid-state supercapacitors, *J. Colloid Interface Sci.*, 2020, **560**, 122–129.
18 X. Jiang, W. Lu, X. D. Yu, S. Y. Song and Y. Xing, Fabrication of a vanadium nitride/N-doped carbon hollow nanosphere composite as an efficient electrode material for asymmetric supercapacitors, *Nanoscale Adv.*, 2020, **2**, 3865–3871.
19 H. Y. Wu, M. L. Qin, Z. Q. Cao, X. L. Li, B. R. Jia and X. H. Qu, Highly efficient synthesis of 2D VN nanoparticles/carbon sheet nanocomposites and their application as supercapacitor electrodes, *Appl. Surf. Sci.*, 2019, **466**, 982–988.
20 S. S. Long, Y. C. Feng, F. L. He, J. Z. Zhao, T. Bai, H. B. Lin, W. L. Cai, C. W. Mao, Y. H. Chen, L. H. Gan, J. Liu, M. D. Ye, X. H. Zeng and M. N. Long, Biomass-derived, multifunctional and wave-layered carbon aerogels toward wearable pressure sensors, supercapacitors and triboelectric nanogenerators, *Nano Energy*, 2021, 85.

Open Access Article. Published on 19 May 2022. Downloaded on 10/22/2025 12:56:45 AM.
This article is licensed under a Creative Commons Attribution-NonCommercial 3.0 Unported Licence.

21 Q. Li, X. J. Tian, W. Yang, L. Q. Hou, Y. Li, B. Jiang, X. Wang and Y. F. Li, Fabrication of porous graphene-like carbon nanosheets with rich doped-nitrogen for high-performance electromagnetic microwave absorption, *Appl. Surf. Sci.*, 2020, 530.

22 A. Fischer, J. O. Muller, M. Antonietti and A. Thomas, Synthesis of ternary metal nitride nanoparticles using mesoporous carbon nitride as reactive template, *ACS Nano*, 2008, **2**, 2489–2496.

23 Y. P. Liu, A. Chatterjee, P. Rusch, C. Q. Wu, P. F. Nan, M. H. Peng, F. Bettels, T. R. Li, C. X. Ma, C. F. Zhang, B. H. Ge, N. C. Bigall, H. Pfnur, F. Ding and L. Zhang, Monodisperse Molybdenum Nanoparticles as Highly Efficient Electrocatalysts for Li-S Batteries, *ACS Nano*, 2021, **15**, 15047–15056.

24 W. P. Ni, Z. X. Liu, Y. Zhang, C. Ma, H. Q. Deng, S. G. Zhang and S. Y. Wang, Electroreduction of Carbon Dioxide Driven by the Intrinsic Defects in the Carbon Plane of a Single Fe-N-4 Site, *Adv. Mater.*, 2021, 33.

25 J. H. Liu, F. F. Li, W. W. Liu and X. Li, Effect of calcination temperature on the microstructure of vanadium nitride/nitrogen-doped graphene nanocomposites as anode materials in electrochemical capacitors, *Inorg. Chem. Front.*, 2019, **6**, 164–171.

26 X. Jiang, W. Lu, Y. Li, Y. Yu, X. Zhou, X. Liu and Y. Xing, An Eco-Friendly Nitrogen Source for the Preparation of Vanadium Nitride/Nitrogen-Doped Carbon Nanocomposites for Supercapacitors, *ChemElectroChem*, 2019, **6**, 3445–3453.

27 B. You, L. Wang, L. Yao and J. Yang, Three dimensional N-doped graphene-CNT networks for supercapacitor, *Chem. Commun.*, 2013, **49**, 5016–5018.

28 X. Li, Y. Tang, J. H. Song, W. Yang, M. S. Wang, C. Z. Zhu, W. G. Zhao, J. M. Zheng and Y. H. Lin, Self-supporting activated carbon/carbon nanotube/reduced graphene oxide flexible electrode for high performance supercapacitor, *Carbon*, 2018, **129**, 236–244.

29 X. H. Li, S. Kurasch, U. Kaiser and M. Antonietti, Synthesis of Monolayer-Patched Graphene from Glucose, *Angew. Chem., Int. Ed.*, 2012, **51**, 9689–9692.

30 H. H. Liu, H. L. Zhang, H. B. Xu, T. P. Lou, Z. T. Sui and Y. Zhang, In situ self-sacrificed template synthesis of vanadium nitride/nitrogen-doped graphene nanocomposites for electrochemical capacitors, *Nanoscale*, 2018, **10**, 5246–5253.

31 X. H. Li, S. Kurasch, U. Kaiser and M. Antonietti, Synthesis of monolayer-patched graphene from glucose, *Angew. Chem., Int. Ed.*, 2012, **51**, 9689–9692.

32 M. Wu, J. M. Yan, X. W. Zhang and M. Zhao, Synthesis of g-C_3N_4 with heating acetic acid treated melamine and its photocatalytic activity for hydrogen evolution, *Appl. Surf. Sci.*, 2015, **354**, 196–200.

33 W. Xing, W. Tu, Z. Han, Y. Hu, Q. Meng and G. Chen, Template-induced high-crystalline g-C_3N_4 nanosheets for enhanced photocatalytic H2 evolution, *ACS Energy Lett.*, 2018, **3**, 514–519.

34 Y. L. Yang, K. W. Shen, Y. Liu, Y. T. Tan, X. N. Zhao, J. Y. Wu, X. Q. Niu and F. Ran, Novel Hybrid Nanoparticles of Vanadium Nitride/Porous Carbon as an Anode Material for Symmetrical Supercapacitor, *Nano-Micro Lett.*, 2017, **9**, 6.

35 Z. Sheng, X. C. Lin, H. Wei, Y. K. Zhang, Z. Tian, C. H. Wang, D. P. Xu and Y. G. Wang, Green synthesis of nitrogen-doped hierarchical porous carbon nanosheets derived from polyvinyl chloride towards high-performance supercapacitor, *J. Power Sources*, 2021, 515.

36 M. R. Pallavolu, Y. A. Kumar, R. R. Nallapureddy, H. R. Goli, A. N. Banerjee and S. W. Joo, In-situ design of porous vanadium nitride@carbon nanobelts: A promising material for high-performance asymmetric supercapacitors, *Appl. Surf. Sci.*, 2022, 575.

37 P. A. Shinde, N. R. Chodankar, S. C. Lee, E. G. Jung, S. Aftab, Y. K. Han and S. C. Jun, All-redox solid-state supercapacitor with cobalt manganese oxide@bimetallic hydroxides and vanadium nitride@nitrogen-doped carbon electrodes, *Chem. Eng. J.*, 2021, 405.

38 G. Sun, H. Ren, Z. Shi, L. Zhang, Z. Wang, K. Zhan, Y. Yan, J. Yang and B. Zhao, V_2O_5/vertically-aligned carbon nanotubes as negative electrode for asymmetric supercapacitor in neutral aqueous electrolyte, *J. Colloid Interface Sci.*, 2021, **588**, 847–856.

39 M. R. Pallavolu, Y. A. Kumar, R. R. Nallapureddy, H. R. Goli, A. N. Banerjee and S. W. Joo, In-situ design of porous vanadium nitride@ carbon nanobelts: A promising material for high-performance asymmetric supercapacitors, *Appl. Surf. Sci.*, 2022, **575**, 151734.

40 P. A. Shinde, N. R. Chodankar, S. Lee, E. Jung, S. Aftab, Y.-K. Han and S. C. Jun, All-redox solid-state supercapacitor with cobalt manganese oxide@ bimetallic hydroxides and vanadium nitride@ nitrogen-doped carbon electrodes, *Chem. Eng. J.*, 2021, **405**, 127029.

41 M. Sethi, U. S. Shenoy and D. K. Bhat, Porous graphene-$NiCo_2O_4$ nanorod hybrid composite as a high performance supercapacitor electrode material, *New J. Chem.*, 2020, **44**, 4033–4041.

42 M. Sethi, U. S. Shenoy and D. K. Bhat, A porous graphene-$NiFe_2O_4$ nanocomposite with high electrochemical performance and high cycling stability for energy storage applications, *Nanoscale Adv.*, 2020, **2**, 4229–4241.

 © 2022 The Author(s). Published by the Royal Society of Chemistry